Tuning the coordination environment of single-atom catalyst M-N-C towards selective hydrogenation of functionalized nitroarenes

Dan Zhou[1,2], Leilei Zhang[2] (✉), Xiaoyan Liu[2], Haifeng Qi[2], Qinggang Liu[2], Ji Yang[2], Yang Su[2], Jingyuan Ma[3], Jianzhong Yin[2] (✉), and Aiqin Wang[2] (✉)

[1] School of Chemical Engineering, State Key Laboratory of Fine Chemicals, Dalian University of Technology, Dalian 116024, China
[2] CAS Key Laboratory of Science and Technology on Applied Catalysis, Dalian Institute of Chemical Physics, Chinese Academy of Sciences, Dalian 116023, China
[3] Shanghai Synchrotron Radiation Facility, Zhangjiang Laboratory (SSRF, ZJLab), Shanghai Advanced Research Institute, Chinese Academy of Sciences, Shanghai 201204, China

ABSTRACT

Fine-tuning of the coordination environment of single-atom catalysts (SACs) is effective to optimize their catalytic performances, yet it remains challenging due to the vulnerability of SACs. Herein, we report a new approach to engineering the coordination environment of M-N-C (M = Fe, Co, and Ni) SACs by using glutamic acid as the N/C source and pyrolysis atmosphere as a regulator. Compared with that in N_2, NH_3 was able to promote the doping of N at $T < 700$ °C yet etch the N-species at higher temperatures, by which the M-N coordination number (CN) and the electronic structure were delicately tuned. It was found that the electron density of Ni single atoms increased with the decrease of Ni-N CN. As a consequence, the capability of Ni-N-C to dissociate H_2 was greatly enhanced and a higher catalytic activity in chemoselective hydrogenation of functionalized nitroarenes was achieved. Moreover, this modulation method could be applied to other transition metals including Fe and Co. In particular, the as-synthesized Co-N-C SAC afforded a turnover frequency of 152.3 h^{-1} with 99% selectivity to 3-vinylaniline in the hydrogenation of 3-nitrostyrene, which was the highest ever reported thus far and was at least one order of magnitude more active than state-of-the-art noble-metal-free M-N-C catalysts, demonstrating the great potential of engineering the coordination environment of SACs.

KEYWORDS

single-atom catalysts, coordination environment, Ni-N-C, chemoselective hydrogenation, pyrolysis atmosphere

1   Introduction

Chemoselective hydrogenation of organic compounds bearing multiple reducible groups is a key transformation in fine chemical industry, which has wide applications in synthesis of pigments, agrochemicals, and pharmaceuticals [1, 2]. For green and sustainable chemical transformations, a nearly 100% selectivity to the target product is highly desired; yet it is often achieved at the cost of turnover numbers in the current catalytic technologies which employ a second component to block or poison the sites for undesired reactions on a nanocatalyst (e.g. Lindlar catalyst) [3]. In order to overcome this "seesaw effect" between the activity and selectivity, single-atom catalysts (SACs) have been designed towards the chemoselective hydrogenations [4–9]. Attributed to the single-atom dispersion of the active metal species, the selective transformations can be sufficiently accomplished in SACs without addition of a second blocking component, thus enabling both high activity and selectivity. For example, Pt_1/FeO_x SAC afforded a selectivity of 98.4% and a TOF of 1,494 h^{-1} for the chemoselective hydrogenation of functionalized nitroarenes under mild reaction conditions (40 °C and 0.3 MPa H_2) [4], which was far superior to the nanocatalysts reported before [10, 11]. Moreover, by tuning the coordination environment of the central Pt single atom

without changing the single-atom dispersion, the activity could be further increased to a TOF of 3,809 h^{-1} while the high chemoselectivity was maintained [12]. These results have demonstrated the unrivalled capability of SACs for chemoselective hydrogenations.

In spite of superior activity of Pt_1/FeO_x SACs, the employment of noble metals raises serious concerns on the sustainability and affordability of the catalyst materials. Therefore, development of non-noble metal catalysts is highly desired [13, 14]. M-N-C (M = Fe, Co, and Ni) materials are a class of promising noble-metal-free catalysts where M coordinates with the surrounding N atoms in the carbon matrix forming strong ionic/covalent bonds [15–18]. The resulting M_1-N_x ($x = 1$–6) entity constitutes unique active sites for a variety of redox reactions, including electrochemical reactions [19–22] and organic transformations [23, 24]. For chemoselective hydrogenation of functionalized nitroarenes, Beller and coworkers firstly reported that, Co_3O_4@N/C and Fe_3O_4@N/C catalysts, which were prepared by pyrolysis of a mixture of metal acetate and 1,10-phenanthroline (phen), were highly selective to the desired anilines for a broad scope of substrates with diverse functional groups [14, 17]. The pioneering work has sparked intensive research interest in this type of catalysts [25, 26]. Nevertheless, the pyrolysis process often produces various M_1-N_x species as

---

well as metallic M nanoparticles and even M oxides/carbides which are encapsulated with carbon layers. The co-existence of diverse species in the M-N-C materials not only undermines the catalyst efficiency, but also poses significant challenge in the identification of genuine active sites. Even if the nanoparticle species can be removed by acid leaching treatment, the left M_1-N_x single-atom species may still not be equally effective in catalysis depending on the exact coordination configuration. Our previous work demonstrated that there were four Fe-N_x (x = 4–6) species in Fe-N-C SACs but only the medium-spin Fe-N_5 species were catalytically active [27]. Similarly, Wu and coworkers found that Co-N_2 species was much more active than Co-N_3 and Co-N_4 analogues [28]. These results suggest that the coordination configuration of M-N_x plays a pivotal role in dictating the catalytic performance, and it critically relies on the preparation conditions including the source of N/C and the pyrolysis temperature/atmosphere [29]. Unfortunately, the lack of fundamental understanding of the pyrolysis process impedes optimization of the preparation parameters towards the modulation of the coordination configurations.

In this work, we report a new method for synthesis of M-N-C SACs by employing glutamic acid as the N/C source, NH_3 as the pyrolysis gas and nanoparticulate silica as the hard template. Through *in situ* monitoring of the tail gas during the pyrolysis process, we found that NH_3 promoted the doping of N into the carbonaceous matrix at a temperature below 700 °C, leading to a higher coordination number (CN) than that under N_2. However, at T > 700 °C, the CN was greatly reduced because of the etching of N-doped carbon by NH_3. Concomitant with the decrease in CN, the capability of M-N-C to activate H_2 was enhanced, leading to improved catalytic efficiency in the chemoselective hydrogenation of functionalized nitroarenes. The turnover frequency (TOF) reached 152.3 h^{-1} (at 80 °C) and 60.2 h^{-1} (at 110 °C) on Co-N-C and Ni-N-C catalysts, respectively, which were among the highest values achieved on non-precious metal catalysts reported thus far.

2 Experimental

2.1 Catalysts preparation

All chemicals were of analytical grade and were used as received without further purification. The typical process for preparation of Ni-N-C SACs is illustrated in Fig. 1(a). Briefly, 0.5 mmol nickel(II) acetate tetrahydrate and 20 mmol glutamic acid were dispersed in 48 mL water, followed by the addition of 2 mL concentrated hydrochloric acid to promote the dissolution of glutamic acid. After a clear and transparent solution was obtained, 1 g nanoparticulate SiO_2 (99.5%, 15 nm, Aladdin) was added, and the mixture was stirred at 60 °C for 4 h. After the solvent was removed by rotary evaporation, the remaining solid was dried at 80 °C overnight, and was subjected to pyrolysis at 800 °C for 2 h in a tubular furnace under NH_3/He (v:v = 7:3, 100 mL·min^{-1}) with a ramp of 5 °C·min^{-1}. The sample was then treated with 10% HF aqueous solution to remove the template SiO_2. The mixture was filtered and washed with water until the filtrate became neutral. The obtained black powder was then dried at 60 °C and denoted as Ni800NH$_3$. Samples prepared under different atmospheres (i.e. NH_3 or N_2) or temperatures were denoted as NiTA (T = temperature, A = atmosphere, for example, Ni800N$_2$). Other transition metal (Fe and Co) based M-N-C SACs were prepared by the same method except for using Fe(OAc)$_2$ or Co(OAc)$_2$ as the metal
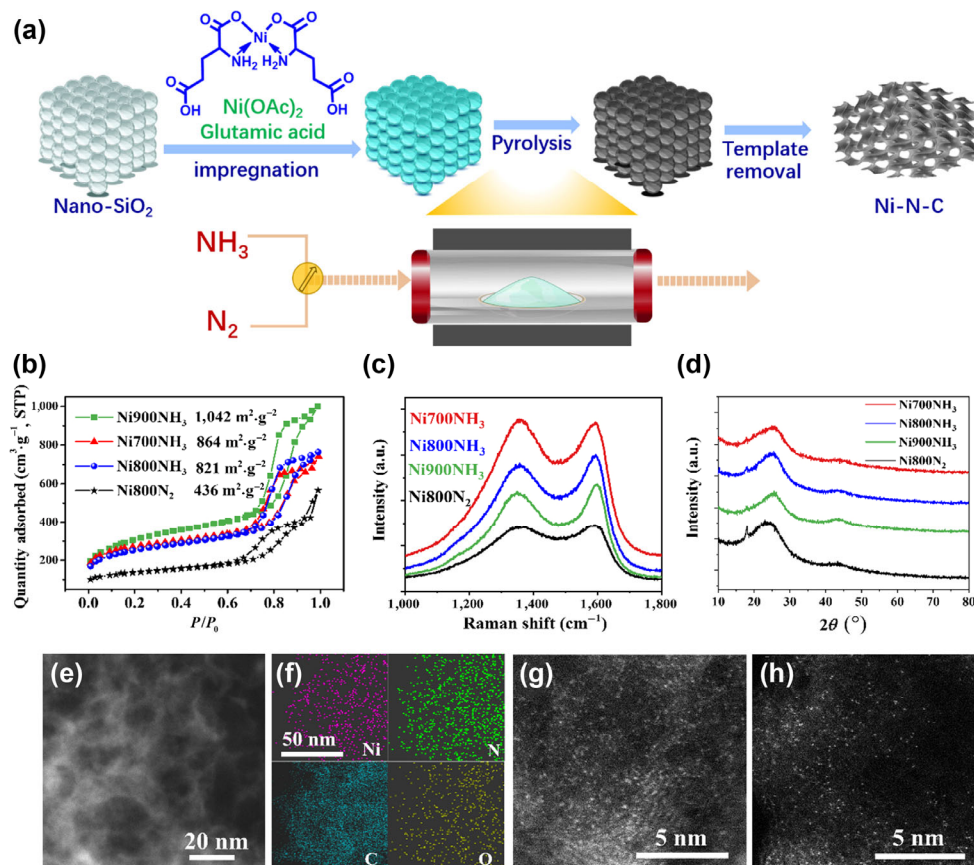
Figure 1 (a) Illustration for preparation of Ni-N-C catalyst. (b)–(d) N_2 adsorption–desorption isotherms, Raman spectra, and XRD patterns of different Ni-N-C catalysts. (e)–(g) scanning transmission electron microscopy (STEM), elemental mapping, and high-angle annular dark-field STEM (HAADF-STEM) images of Ni800NH$_3$. (h) HAADF-STEM image of Ni900NH$_3$.

precursors. For comparison, Ni(phen)800NH₃ and Ni(phen)800N₂ were prepared by employment of 1,10-phenanthroline (phen) to replace glutamic acid. Ni800NH₃-H₂ was obtained by subjecting the Ni800NH₃ to a second treatment in H₂ at 400 °C for 1 min.

2.2 Catalytic activity tests

The hydrogenation reaction of nitroarenes was carried out in a 10 mL Teflon-lined autoclave equipped with a magnetic stirring system. Typically, 0.565 mmol 3-nitrostyrene (NS), 20 mg of a Ni-N-C catalyst, 0.25 mmol o-xylene (as an internal standard) and 2 mL methanol (as solvent) were mixed in the autoclave. Then the reactor was sealed and flushed with N₂ several times, followed by charging with 3 MPa H₂. To start the reaction, the autoclave was put in a thermostatic water bath and heated at 80 °C and the reaction mixture was continuously stirred with a stirring speed of 1,200 rpm. After the reaction, the liquid was separated from the solid catalyst and then subjected to gas chromatograpyhy (GC) analysis. Before the measurements of the intrinsic catalytic activities of the catalysts, the mass transport limitations were carefully excluded by studying the effects of agitation speed and catalyst loading on the reaction rate (Figs. S1 and S2 in the Electronic Supplementary Material (ESM)). The kinetic experiments were performed by controlling the NS conversion below 30%, and the TOF was calculated based on the initial reaction rate (conversion < 30%) according to the formula of

$$TOF = \frac{\text{moles of NS consumed}}{\text{moles of metal} \times \text{reaction time}}$$

For measurements of the reaction order respect to H₂, 5 points of pressure were selected, which were 1, 2, 3, 4, and 5 MPa, respectively, and the concentration of NS was set as 0.36 mol·L⁻¹. For measurements of the reaction order respect to NS, the concentrations of NS were 0.12, 0.2, 0.29, 0.36, and 0.48 mol·L⁻¹, and the pressure of H₂ was kept at 3 MPa.

3 Results and discussion

3.1 Formation of single-atom Ni-N-C catalysts

Single-atom Ni-N-C catalysts were prepared by high temperature pyrolysis of a mixture of nickel acetate and glutamic acid under inert or NH₃ atmosphere (Fig. 1(a)). Glutamic acid was selected as N, O-bidentate ligand of Ni(II) considering that the easy decomposition of carboxyl group into CO/CO₂ at high temperatures will provide opportunity for tuning the coordination environment of Ni(II). SiO₂ nanoparticles were employed as the hard template to increase the surface area of the catalysts and the accessibility of Ni single atoms. It was found that the pyrolysis atmosphere imposed a great impact

on the textural properties of the yielded materials; pyrolysis in NH₃ atmosphere led to almost two-fold increase in the surface area, along with the enlargement of pore volume and pore size compared with that in N₂ (Fig. 1(b), Fig. S3 and Table S1 in the ESM), which could be attributed to higher etching capability of NH₃. Raman spectra of these catalysts (Fig. 1(c)) display two bands at 1,356 and 1,593 cm⁻¹, corresponding to disordered sp³ carbon (D) and graphitic sp² (G), respectively [30]. The intensity ratio of D to G band (I_D/I_G) decreased from 1.02 to 0.92 with an increase in the pyrolysis temperature in NH₃, suggesting higher temperatures promote graphitization of the carbon backbone, possibly by etching the amorphous carbon atoms [31, 32].

The X-ray diffraction (XRD) patterns of the series of Ni-N-C catalysts did not show any diffraction peak assigned to Ni-containing crystal phase (Fig. 1(d)), indicating Ni species are highly dispersed. In line with the XRD result, nonanoparticles of metallic Ni or Ni oxides were observed in low-magnification transmission electron microscopy (TEM) images (Fig. 1(e) and Fig. S4 in the ESM), and the Ni, N, and O signals were well dispersed and coincided in the elemental mapping images by energy-dispersive X-ray spectroscopy (EDX, Fig. 1(f)), suggesting that the Ni-species are probably coordinated with N/O atoms and highly dispersed in the carbon matrix. The atomic dispersion of Ni species was visualized by sub-Ångström-resolution HAADF-STEM (AC-HAADF-STEM) images, which clearly show a large number of uniformly dispersed Ni single atoms (Fig. 1(g)) in the carbon matrix. Examination of different regions excluded the existence of Ni clusters. Notably, even in the sample pyrolyzed at a temperature as high as 900 °C, the Ni species still existed as single atoms (Fig. 1(h)). However, when glutamic acid was replaced by an O, O-bidentate ligand (e.g. glutaric acid), dramatic aggregation took place during pyrolysis, leading to the formation of Ni nanoparticles with sizes bigger than 10 nm (Fig. S5 in the ESM). This result strongly suggests that the N atoms in the glutamic acid are critical to the stabilization of Ni single atoms through forming strong ionic/covalent bonds, and in good agreement with our previous results [33].

To get insight into the pyrolysis process under N₂ or NH₃ atmosphere, the tail gas was online monitored (Fig. 2). Under N₂ atmosphere, CO₂ was the main gaseous product below 500 °C, which arose from the decarboxylation of glutamic acid (Scheme S1 in the ESM, Eq. 1) [34]. Above 500 °C, H₂O and NH₃ were produced as a result of intra-/inter-molecular condensation of glutamic acid and cyclization/dimerization of amino acid (Scheme S1 in the ESM, Eqs. 2 and 3), respectively, and the latter reactions could account for the formation of pyridine and pyrrolic N species. When the temperature was raised to above 700 °C, a small amount of HCN was detected as a result of decomposition of heterocylic-N species (Scheme
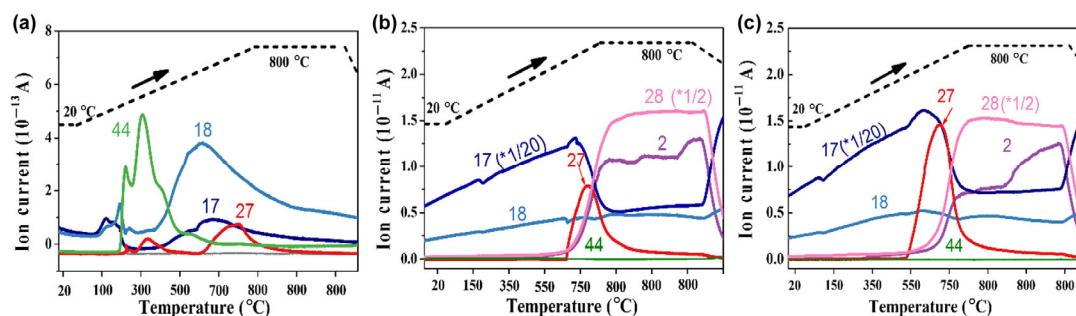
Figure 2 Monitoring results of the tail gas by mass spectrometry (MS) during pyrolysis of Ni-Glu/SiO₂ ((a) and (b)) and Glu/SiO₂ (c) under different atmosphere: (a) He, and (b) and (c) NH₃. The signals with *m/z* of 2 (H₂), 17 (NH₃), 18 (H₂O), 27 (HCN), 28 (N₂ or CO), and 44 (CO₂) were monitored as a function of the pyrolysis temperature.

S1 in the ESM, Eq. 4) [35], which can be responsible for the partial loss of N content at high temperatures. In contrast to inert atmosphere, the pyrolysis in NH₃ involves quite different reactions. H₂O emerged as the main gas product at $T < 700$ °C, which came from the intra-/inter-molecular condensation of glutamic acids with NH₃ yielding amides (Scheme S1 in the ESM, Eqs. 5–7) [36]. Such condensation reactions will be favourable to the doping of N atoms into the carbon backbone (e.g. Eq. 7). Notably, the signal intensity of H₂O was much higher than that under N₂ atmosphere, implying the reaction between NH₃ and –COOH in glutamic acid dominated the process. Quite different from the pyrolysis in N₂, no CO₂ was detected at $T < 700$ °C, indicating decarboxylation reactions did not take place under NH₃ atmosphere. At $T > 700$ °C, HCN began to form and reached maximum at about 780 °C. The amount of HCN produced in NH₃ was much more than that under N₂, suggesting the etching of amorphous C and N atoms also occurred besides the decomposition of heterocylic-N (Scheme S1 in the ESM, Eqs. 8–10) [37]. The detection of CO rather than CO₂ at $T > 700$ °C further suggests the occurrence of reaction 10. Based on the analysis result of the pyrolysis tail gas, it can be reasonably concluded that at $T \leq 700$ °C, there should be more amount of N doped into the carbon matrix when the pyrolysis proceeds in NH₃, whereas at $T > 700$ °C, the N content would be reduced due to the high capability of NH₃ for etching amorphous C and N atoms. Interestingly, it was also found that the presence of Ni(II) made the temperature for producing HCN increased by ~ 100 °C (Fig. 2(b) vs. 2(c)), suggesting the strong coordination of Ni(II) with N atoms alleviates the loss of N under NH₃.

3.2 Probing into the electronic and coordination structures of Ni single atom

For SACs, the coordination environment of single atoms plays a pivotal role in dictating the catalytic performance, which is resembling the role of organic ligands in organometallic catalysts [38]. In order to probe into the coordination structure of the Ni single atoms, X-ray photoelectron spectroscopy (XPS) and X-ray absorption spectroscopy (XAS) were performed on the series of Ni-N-C catalysts. Figure 3 displays Ni 2p and N 1s XPS of different Ni-N-C samples. The binding energy of Ni 2p₃/₂ at ~ 855.0 eV suggested the oxidation state of Ni single atoms was between Ni(0) and Ni(II) [39, 40], most likely being Ni(I) according to Liu and coworkers [41], and it shifted negatively in the order of Ni700NH₃ (855.2 eV) > Ni800NH₃ (854.9 eV) = Ni900NH₃ (854.9 eV) > Ni800NH₃-H₂ (854.6 eV). This result suggests that the electron density of Ni single atoms slightly increased with the elevation of pyrolysis temperature, and the rapid treatment with H₂ could further increase the electron

density of Ni single atom. It is also noted that the pyrolysis atmosphere (N₂ or NH₃) did not cause remarkable difference in the oxidation state of Ni single atoms. On the other hand, the N 1s XPS spectra were deconvoluted into five peaks with binding energy at 398.5, 399.8, 401.1, 403.3, and 405.2 eV, which can be assigned to pyridinic N, N-Ni moiety, pyrrolic N, graphitic N, and oxidized graphitic N, respectively (Fig. 3(b) and Table S2 in the ESM) [42, 43]. The surface compositions of these samples determined by XPS are summarized in Table 1. All the samples were composed of Ni, N, C, and O elements, but their relative contents were quite different depending on the pyrolysis temperature and atmosphere. The N concentration in the Ni700NH₃ sample was as high as 16.1 at.%, however, it decreased dramatically to 8.9 at.% and 6.4 at.% with an increase in pyrolysis temperature to 800 and 900 °C, respectively. When the sample Ni800NH₃ was treated by H₂, the N content was further reduced to 8.5 at.%. This trend was in good agreement with the aforementioned pyrolysis mechanism in NH₃, substantiating that NH₃ promoted the doping of N into carbon matrix at ~ 700 °C whereas the removal of N at higher temperatures. Moreover, it was noticed that both the pyridinic N and N-Ni concentrations decreased markedly whereas the pyrrolic and graphitic N concentrations increased with the elevation of the pyrolysis temperature, which suggests that NH₃ etching mainly occurs at the pyridinic N species and the Ni single atoms coordinate with pyridinic N. In contrast to the pyrolysis in NH₃, the N content decreased smoothly from 9.7 at.% to 6.7 at.% with an increase of temperature from 700 to 900 °C under N₂ atmosphere, and the relative contents of various N species did not change much, reflecting different reaction mechanism from that in NH₃.

For the surface Ni concentration, it decreased from 0.63 at.% to 0.46 at.% when the temperature raised from 700 to 800 °C under NH₃ atmosphere, and then levelled off with a further increase of temperature to 900 °C or when treated by H₂. The decrease of Ni content with an increase of pyrolysis temperature was most likely due to the aggregation of Ni single atoms at higher temperature and the subsequent removal of these aggregates by acid treatment. On the contrary, the surface Ni content increased monotonically with pyrolysis temperature under N₂ atmosphere due to the loss of carbon, implying that the Ni single atoms are more stable against aggregation in N₂ than in NH₃, which was further corroborated by the STEM images of the as-pyrolyzed sample in N₂ (Fig. S6 in the ESM). Based on the surface content of N-Ni moiety as well as the total Ni and N contents, we can calculate the surface N/Ni ratio in the Ni-N coordination sphere, which corresponds to the surface CN(CN_XPS) of Ni-N shell. As shown in Table 1, under NH₃ atmosphere, the Ni-N CN_XPS decreased remarkably
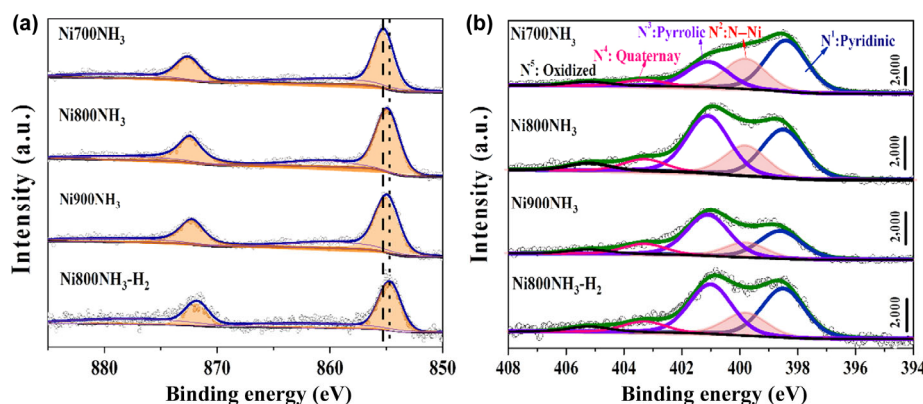
Figure 3 XPS spectra of Ni 2p (a) and N1s (b) for different Ni-N-C single atom catalysts.

Table 1 Surface composition of different Ni-N-C catalysts determined by XPS measurements

| Catalyst | Ni (at.%) | C (at.%) | O (at.%) | N[a] | | | | | | Ni-N CN_{XPS}[b] |
				Total (at.%)	N^1 (area%)	N^2 (area%)	N^3 (area%)	N^4 (area%)	N^5 (area%)	
$Ni700NH_3$	0.63	79.3	3.9	16.1	43.7	26.1	21.7	5.2	3.3	6.7
$Ni800NH_3$	0.46	86.6	3.7	8.9	36.6	18.3	32.0	8.4	4.6	3.5
$Ni900NH_3$	0.47	90.3	2.6	6.4	31.4	10.5	43.4	10.4	4.3	1.4
$Ni800NH_3$-H_2	0.46	87.6	3.2	8.5	35.7	16.4	35.9	8.0	4.0	3.0
$Ni700N_2$	0.51	83.0	4.2	9.7	38.9	13.0	38.4	6.9	2.9	2.5
$Ni800N_2$	0.62	86.3	4.7	8.0	35.6	16.3	37.9	6.8	3.4	2.1
$Ni900N_2$	0.74	85.6	4.8	6.1	30.8	14.1	40.8	9.7	4.6	1.2

[a] N^1, N^2, N^3, N^4, and N^5 represent pyridinic N, N-Ni moiety, pyrrolic N, graphitic N, and oxidized graphitic N, respectively (see Fig. 3(b)). [b] Ni-N CN_{XPS} was calculated by area% of $N^2 \times N_{total}$ (at.%)/Ni (at.%).

from 6.7 to 3.6 with an increase of the pyrolysis temperature from 700 to 800 °C, and further decreased to 3.0 when sample $Ni800NH_3$ was further treated in H_2. For comparison, the Ni-N CN_{XPS} only slightly reduced from 2.5 at 700 °C to 2.1 at 800 °C when the pyrolysis was performed in N_2. These results demonstrate that the coordination environment of Ni single atoms can be effectively modulated by changing the pyrolysis temperature and atmosphere.

The X-ray absorption fine structure (XAFS) characterization was also conducted to determine the electronic and coordinative structure of Ni single atoms. The Fourier-transformed k^2-weighted extended XAFS (EXAFS) spectra in *R*-space are shown in Fig. S7 in the ESM. The Ni foil reference displayed a predominant peak at 2.2 Å, which was assigned to the Ni–Ni contribution. By contrast, no peak was observed at the same position for the Ni-N-C catalysts, thus precluding the existence of Ni–Ni bond and being consistent with XRD and HAADF-STEM characterization results. On the other hand, all of the Ni-N-C samples gave a single peak at ~ 1.5 Å, suggesting Ni single atoms in these samples are coordinated to N/O atoms. It should be pointed out that it is difficult to discriminate the Ni-N and Ni-O coordination here due to the similar atomic number of N and O [44, 45]. The intensity of the Ni-N/O peak decreased in the order of $Ni700NH_3$ > $Ni900NH_3$ > $Ni800NH_3$ > $Ni800NH_3$-H_2 (inset in Fig. S7 in the ESM), indicating the decreased CN. Table 2 summarizes the fitting results of the EXAFS data. It is noted that the Ni-N CN provided by EXAFS characterization (CN_{EXAFS}) is well consistent with the trend given by XPS technique although the exact CNs determined by two different techniques are different to some extent. Such deviation arises probably from the bulk and surface characterization methods which will be discussed later.
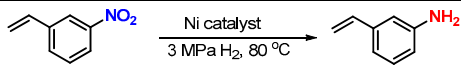
Table 2 The best-fitted EXAFS results of Ni-N-C catalysts[a]

Sample	Shell	CN	σ^2 (10^{-2} Å)	R (Å)	ΔE_0 (eV)	R factor
Ni foil	Ni-Ni	12	0.6	2.48	4.5	0.001
$Ni700NH_3$	Ni-N	3.9	0.6	1.85	−13.7	0.002
$Ni800NH_3$	Ni-N	3.6	0.5	1.85	−14.4	0.002
$Ni900NH_3$	Ni-N	3.7	0.6	1.85	−14.1	0.002
$Ni800NH_3$-H_2	Ni-N	3.2	0.5	1.84	−16.1	0.001

[a] CN is the coordination number for the absorber–backscatterer pair, R is the average absorber–backscatterer distance, σ^2 is the Debye-Waller factor, and ΔE_0 is the inner potential correction. The accuracy of the above parameters is estimated as CN, ±20%; R, ±1%; σ^2, ± 20%; ΔE_0, ±20%. The data range used for data fitting in *R*-space and *k*-space (Δk) are 1.0–1.8 Å and 3.6–12.1 Å^{-1}, respectively.

3.3 Catalytic performance

The hydrogenation of NS was employed as the probe reaction to evaluate the catalytic performance of these catalysts. Our blank tests revealed that either $Ni(OAc)_2$ or complex of $Ni(OAc)_2$ and glutamic acid was inactive at typical reaction conditions (3 MPa H_2, 80 °C). Only when the Ni-N precursor was pyrolyzed at or above 700 °C, was the derived materials able to catalyze the hydrogenation reaction. It was interesting to find that the activity was highly dependent on the pyrolysis atmosphere and temperature. Pyrolysis in NH_3 produced much more active catalysts than in N_2 irrespective of the N/C source (Table 3), which could be ascribed to the higher surface area and/or hierarchical pores of the former leading to the improved accessibility of the single-atom sites. Subsequent treatment with H_2 at mild conditions following the pyrolysis in NH_3 resulted in a further increase in activity. For the series of catalysts derived from pyrolysis under NH_3 but at different temperatures, the $Ni800NH_3$ afforded the highest TOF of 29.4 h^{-1}, which was three-fold higher than that over the $Ni700NH_3$. We also found that the N/C source imposed a significant effect on the catalytic activity. When 1,10-phenanthroline and lysine were used as the N/C source, the resultant $Ni(phen)800NH_3$ and $Nilysine800NH_3$ catalysts delivered TOFs of only 12.3 and 13.1 h^{-1}, respectively, which were much lower than that over the $Ni800NH_3$ catalyst. In light of superior activity of the $Ni800NH_3$ catalyst, we investigated the effects of reaction temperature and time. As shown in Fig. S8 in the ESM, the NS conversion attained 100% after 9 h reaction at 80 °C and no byproducts were detected during the whole reaction period. Even if at a relatively higher temperature (e.g. 110 °C), the selectivity remained > 99% while the TOF was enhanced from 29.4 to 60.2 h^{-1} (entry 6, Table 3), demonstrating the unique advantage of single-atom Ni-N_x species in affording both high activity and selectivity, which is usually difficult to access by the noble-metal NPs catalysts [46, 47]. The high activity of the $Ni800NH_3$ was also demonstrated by its ability to catalyze the reaction even at room temperature (25 °C), affording a conversion of 81.3% after reaction for 36 h (entry 17). To our knowledge, this is the first report that M-N-C non-noble-metal catalyst can catalyze the hydrogenation reaction at room temperature. Moreover, the present synthesis strategy could be extended to other transition metals such as Fe-N-C and Co-N-C SACs (Fig. S9 in the ESM). In particular, the as-synthesized Co-N-C catalysts were much more active than Fe-N-C and Ni-N-C catalysts, with $Co800NH_3$ as the most active non-noble metal catalyst reported thus far, delivering a TOF as high as 152.3 h^{-1} (entry 12). When compared with the non-noble

Table 3 Catalytic performances of different catalysts in the hydrogenation reaction of NS*

$$\text{NO}_2\text{-styrene} \xrightarrow[\text{3 MPa H}_2,\ 80\ °C]{\text{Ni catalyst}} \text{NH}_2\text{-styrene}$$

Entry	Catalyst	Time (min)	Conv. (%)	Select. (%)	TOF (h⁻¹)[a]
1	Ni700NH₃	60	24.3	> 99	8.5
2	Ni800NH₃	20	15.2	> 99	29.4
3	Ni900NH₃	30	14.9	> 99	21.0
4	Ni800N₂	60	23.2	> 99	8.2
5	Ni800NH₃-H₂	15	10.5	> 99	37.6
6[b]	Ni800NH₃	30	17.2	> 99	60.2
7	Ni(phen)800N₂	60	13.1	> 99	6.0
8	Ni(phen)800NH₃	50	19.9	> 99	12.3
9	Nilysine800N₂	90	19.0	> 99	7.2
10	Nilysine800NH₃	60	22.1	> 99	13.1
11	Co800N₂	30	12.6	> 99	18.9
12	Co800NH₃	10	24.4	> 99	152.3
13	Co700NH₃	10	17.5	> 99	59.3
14	Co900NH₃	10	28.8	> 99	136.0
15[c]	Fe800N₂	480	0	> 99	—
16[c]	Fe800NH₃	480	25.6	> 99	3.5
17[d]	Ni800NH₃	2160	81.3	> 99	—

*Notes: Reaction conditions: methanol (2 mL), 3 MPa H_2, 80 °C. The conversion and selectivity were determined by GC. Detailed data for the calculation of the TOFs are listed in Table S4 in the ESM. [a]All the TOF values were calculated based on the initial reaction rates which were measured at the kinetically controlled regime by keeping the substrates conversions below 30%. [b]110 °C, NS (2 mmol). [c]110 °C. [d]Room temperature (25 °C).

metal catalysts reported in literature (Table S3 in the ESM), it can be found that our Ni800NH₃ and Co800NH₃ were several times to one order of magnitude more active, and even comparable to some noble metal NPs catalysts [48] while keeping 100% selectivity to the target product, demonstrating the superiority of our synthesis method to other approaches.

In addition to superior activity, the Ni800NH₃ catalyst was well tolerant to various substrates with different functional groups, such as chlorides, bromides, and ketone, and good to excellent yields of the corresponding products were obtained without dehalogenation or over-hydrogenation side-reactions (Table S5 in the ESM). In addition, the catalyst could be easily recovered by centrifugation or filtration, and could be reused for at least 5 times without obvious decrease in conversion or selectivity (Fig. S10 in the ESM). The HAADF-STEM images of the used catalyst show that Ni still existed as single atoms without aggregation (Fig. S11 in the ESM), and XPS results suggest that the electronic structures of both N and Ni remained essentially unchanged after the reaction (Fig. S12 in the ESM), demonstrating the high durability of the catalyst.

### 3.4　Structure-activity relationship

For SACs, metal single atoms are coordinated with N/C/O containing electron-withdrawing groups via covalent/ionic bonding interactions [6], and the resultant coordination sphere (first and second) can be regarded as a catalytic entity to govern the activity/selectivity, which resembles the organometallic analogues. Therefore, tuning the local coordination structure of metal single atoms can be an effective avenue towards

tuning the catalytic performance [49]. In our previous work [12], by using Pt-O CN as a descriptor of Pt single atoms on FeO$_x$ support, we successfully established the structure-activity relationship: the activity increases linearly with the decrease of Pt-O CN. In this work, in order to establish the relationship between activity and the coordination environment of Ni single-atom sites, we plotted the TOFs as a function of Ni-N CN which was determined by both XPS and EXAFS, as shown in Fig. 4. It can be clearly seen that the activity monotonically increased with a decrease of the Ni-N CN$_{EXAFS}$ and arrived at the highest value at Ni-N CN$_{EXAFS}$ of ~ 3, and concomitantly, the binding energy of Ni 2p$_{3/2}$ decreased (Fig. 4(b)). This trend implies that the hydrogenation activity is closely correlated with the electronic structure of Ni single atoms [50], and the latter is largely determined by its local coordination structure. Such a trend is also in good agreement with what was found in Pt₁/Fe₂O₃ system in our previous report [12], corroborating that the first-shell CN of Ni single atoms can be a suitable descriptor of the electronic and catalytic properties. We also noted that when the surface Ni-N CN$_{XPS}$ determined by XPS was used as the descriptor, the TOF curve presented a volcano shape with the peak appearing at Ni-N CN$_{XPS}$ of ~ 3. The deviating point was caused by Ni900NH₃ sample which had a much lower Ni-N CN$_{XPS}$ (1.4 determined by XPS) than Ni-N CN$_{EXAFS}$ (3.7 determined by EXAFS). Taking into account that the Ni single-atom species in the Ni900NH₃ sample had almost the same oxidation state as that in the Ni800NH₃ and there were more pyridinic N species etched by NH₃ at 900 °C (Fig. 3 and Table 1), we can reasonably postulate that the coordinatively unsaturated Ni-N₂ structure is probably formed at 900 °C; however, it is subject to being saturated by adsorption of oxygen upon it being exposed to ambient atmosphere, forming the 2O₂-Ni-N₂-like structure, which has a Ni-N(O, C) CN$_{EXAFS}$ of close to 4 measured by EXAFS. On the other hand, the much bigger CN determined by XPS than that by EXAFS for the Ni700NH₃ is most likely due to the favorable N-doping during the pyrolysis in NH₃ at or below 700 °C, which enriches N on the surface instead of in bulk. It is of importance that both XPS and EXAFS consistently determined the Ni-N CN of ~ 4 and ~ 3 for Ni800NH₃ and Ni800NH₃-H₂, respectively, suggesting their local structures of Ni-N₄ and Ni-N₃. Moreover, the Ni-N₃ sites were slightly more active than Ni-N₄ due to the more electron-rich Ni single atoms in the former. Bao and coworkers reported that coordinatively unsaturated Ni-N₃ was more active than Ni-N₄ for electro-reduction of CO₂ [51]; and Li and coworkers stated that the Ni-N₃ structure was the most active site for the selective hydrogenation of nitroarenes due to its favourable activation for –NO₂ group [43], although the TOF value they reported was one order of magnitude lower than our present work (Table S3 in the ESM).

In our earlier work regarding the Ni-N-C SAC synthesized by pyrolysis of Ni(phen)₃ in N₂, we obtained Ni-N₅ structure which could activate H₂ heterolytically [33]. In this work, Ni700NH₃ had a Ni-N₆ structure on the surface based on XPS analysis and its hydrogenation activity was lower than the Ni800NH₃ by a factor of 2. In order to understand the mechanism behind such a large activity difference, we performed kinetic studies and H₂–D₂ exchange experiments. As shown in Fig. 5, the reaction order with respect to H₂ and NS was measured to be 0.6 and 1.0, respectively. The reaction order close to 0.5 with respect to H₂ pressure suggested the heterolysis of H₂ into H⁺ and H⁻, and the electrophilic attack of H⁺ to –NO₂ group was involved in the rate-determining step [52]. It is interesting to note that the reaction order with respect to H₂ was 0.4 and 1.2 for Co800NH₃ and Fe800NH₃ (Fig. S13 in the ESM),
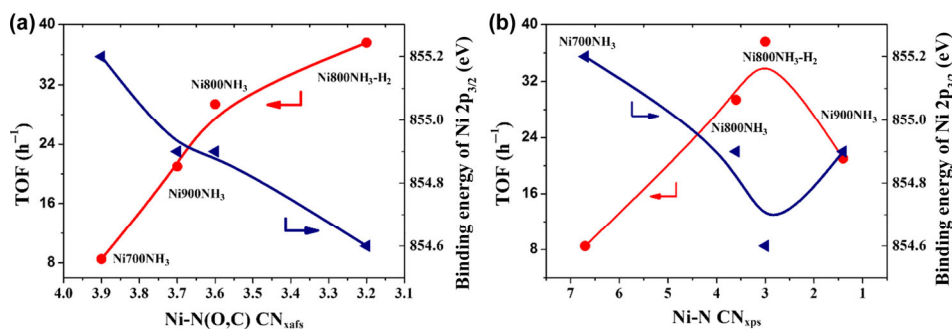
Figure 4 Relationship between TOF and Ni oxidation state against the CN of Ni-N determined by EXAFS (a) and XPS (b).
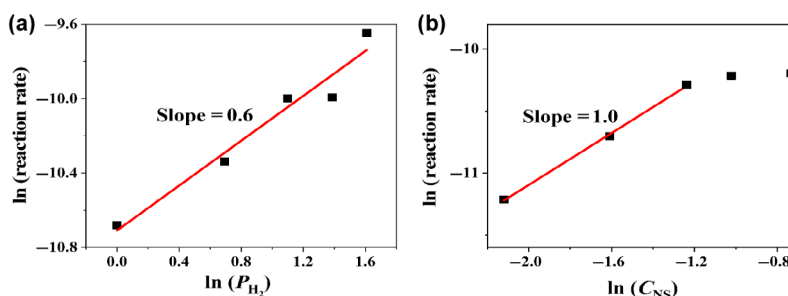
Figure 5 Dependences of reaction rate on H_2 pressure (a) and NS (b). Reaction conditions: (a) the concentration of NS was kept at 0.36 mol·L^{-1}, P_{H_2} = 1–5 MPa; (b) P_{H_2} = 3 MPa, the concentration of NS was varied in the range of 0.12–0.48 mol·L^{-1}. In all the kinetic measurements, the conversions were kept below 30%.

respectively, which is in good agreement with the activity order of $Co800NH_3 > Ni800NH_3 > Fe800NH_3$, indicating H_2 activation and dissociation is the rate-determining step for these M-N-C SACs.

The H–D exchange profiles (Fig. 6) show that the HD signal over the $Ni800NH_3$ catalyst began to appear at above 70 °C and increased sharply with the reaction temperature, which is in stark contrast with the undetectable H–D exchange activity below 250 °C over the $Ni700NH_3$ catalyst. This result indicates that the high activity of $Ni800NH_3$ catalyst for nitrostyrene hydrogenation can be attributed to its superior capability to activate H_2. Compared with $Ni800NH_3$, the Ni center in the $Ni800NH_3$-H_2 was more electron-rich, which would activate H_2 with a lower energy barrier through donating electron to the antibonding orbit of H_2 molecule [53], thus accounting for its higher hydrogenation activity.
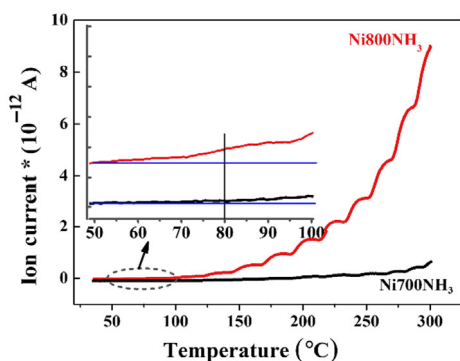
Figure 6 H–D exchange profiles (HD: m/z = 3) of the catalysts calcined at different temperatures.

4 Conclusions

In summary, we have developed a new approach to modulate the coordination environment of M-N-C SACs. By pyrolysis of Ni(II)-glutamic acid complex under NH_3 atmosphere at 700–900 °C, both the local coordination environment and the

electronic properties could be finely tuned through changing the pyrolysis atmosphere and temperature. An interesting trend was obtained: The Ni-N CN decreased with the pyrolysis temperature rising from 700 to 800 °C, and concurrently, the electron density of Ni single atoms became increased. Further treatment with H_2 could result in more electron-rich Ni single-atom centers. As a consequence, the catalytic activity for selective hydrogenation of substituted nitroarenes was increased following this trend without compromising the chemoselectivity. This modulating method could be also extended to Fe and Co. In particular for the as-synthesized Co-N-C, the activity was one order of magnitude higher than the state-of-the-art M-N-C catalysts reported to date. Our work opens a vision to engineer the coordination environment of other SACs for the chemoselective hydrogenation reactions.

References

[1] Downing, R. S.; Kunkeler, P. J.; van Bekkum, H. Catalytic syntheses of aromatic amines. *Catal. Today* **1997**, *37*, 121–136.

[2] Macino, M.; Barnes, A. J.; Althahban, S. M.; Qu, R. Y.; Gibson, E. K.; Morgan, D. J.; Freakley, S. J.; Dimitratos, N.; Kiely, C. J.; Gao, X. et al. Tuning of catalytic sites in Pt/TiO_2 catalysts for the

chemoselective hydrogenation of 3-nitrostyrene. *Nat. Catal.* **2019**, *2*, 873–881.

[3] Zhang, L. L.; Zhou, M. X.; Wang, A. Q.; Zhang, T. Selective hydrogenation over supported metal catalysts: From nanoparticles to single atoms. *Chem. Rev.* **2020**, *120*, 683–733.

[4] Wei, H. S.; Liu, X. Y.; Wang, A. Q.; Zhang, L. L.; Qiao, B. T.; Yang, X. F.; Huang, Y. Q.; Miao, S.; Liu, J. Y.; Zhang, T. FeOₓ-supported platinum single-atom and pseudo-single-atom catalysts for chemoselective hydrogenation of functionalized nitroarenes. *Nat. Commun.* **2014**, *5*, 5634.

[5] Yang, X. F.; Wang, A. Q.; Qiao, B. T.; Li, J.; Liu, J. Y.; Zhang, T. Single-atom catalysts: A new frontier in heterogeneous catalysis. *Acc. Chem. Res.* **2013**, *46*, 1740–1748.

[6] Wang, A. Q.; Li, J.; Zhang, T. Heterogeneous single-atom catalysis. *Nat. Rev. Chem.* **2018**, *2*, 65–81.

[7] Liu, W. P.; Zhang, L. L.; Yan, W. S.; Liu, X. Y.; Yang, X. F.; Miao, S.; Wang, W. T.; Wang, A. Q.; Zhang, T. Single-atom dispersed Co-N-C catalyst: Structure identification and performance for hydrogenative coupling of nitroarenes. *Chem. Sci.* **2016**, *7*, 5758–5764.

[8] Zhang, L. L.; Ren, Y. J.; Liu, W. G.; Wang, A. Q.; Zhang, T. Single-atom catalyst: A rising star for green synthesis of fine chemicals. *Natl. Sci. Rev.* **2018**, *5*, 653–672.

[9] He, X. H.; He, Q.; Deng, Y. C.; Peng, M.; Chen, H. Y.; Zhang, Y.; Yao, S. Y.; Zhang, M. T.; Xiao, D. Q.; Ma, D. et al. A versatile route to fabricate single atom catalysts with high chemoselectivity and regioselectivity in hydrogenation. *Nat. Commun.* **2019**, *10*, 3663.

[10] Boronat, M.; Concepción, P.; Corma, A.; González, S.; Illas, F.; Serna, P. A molecular mechanism for the chemoselective hydrogenation of substituted nitroaromatics with nanoparticles of gold on TiO₂ catalysts: A cooperative effect between gold and the support. *J. Am. Chem. Soc.* **2007**, *129*, 16230–16237.

[11] Serna, P.; Boronat, M.; Corma, A. Tuning the behavior of Au and Pt catalysts for the chemoselective hydrogenation of nitroaromatic compounds. *Top. Catal.* **2011**, *54*, 439–446.

[12] Ren, Y. J.; Tang, Y.; Zhang, L. L.; Liu, X. Y.; Li, L.; Miao, S.; Su, D. S.; Wang, A. Q.; Li, J.; Zhang, T. Unraveling the coordination structure-performance relationship in Pt₁/Fe₂O₃ single-atom catalyst. *Nat. Commun.* **2019**, *10*, 4500.

[13] Ren, Y. J.; Wei, H. S.; Yin, G. Z.; Zhang, L. L.; Wang, A. Q.; Zhang, T. Oxygen surface groups of activated carbon steer the chemoselective hydrogenation of substituted nitroarenes over nickel nanoparticles. *Chem. Commun.* **2017**, *53*, 1969–1972.

[14] Jagadeesh, R. V.; Surkus, A. E.; Junge, H.; Pohl, M. M.; Radnik, J.; Rabeah, J.; Huan, H.; Schünemann, V.; Brückner, A.; Beller, M. Nanoscale Fe₂O₃-based catalysts for selective hydrogenation of nitroarenes to anilines. *Science* **2013**, *342*, 1073–1076.

[15] Zhang, L. L.; Wang, A. Q.; Wang, W. T.; Huang, Y. Q.; Liu, X. Y.; Miao, S.; Liu, J. Y.; Zhang, T. Co-N-C catalyst for C–C coupling reactions: On the catalytic performance and active sites. *ACS Catal.* **2015**, *5*, 6563–6572.

[16] Chen, F.; Surkus, A. E.; He, L.; Pohl, M. M.; Radnik, J.; Topf, C.; Junge, K.; Beller, M. Selective catalytic hydrogenation of heteroarenes with *N*-graphene-modified cobalt nanoparticles (Co₃O₄-Co/NGr@α-Al₂O₃). *J. Am. Chem. Soc.* **2015**, *137*, 11718–11724.

[17] Westerhaus, F. A.; Jagadeesh, R. V.; Wienhöfer, G.; Pohl, M. M.; Radnik, J.; Surkus, A. E.; Rabeah, J.; Junge, K.; Junge, H.; Nielsen, M. et al. Heterogenized cobalt oxide catalysts for nitroarene reduction by pyrolysis of molecularly defined complexes. *Nat. Chem.* **2013**, *5*, 537–543.

[18] Chen, Y. J.; Ji, S. F.; Chen, C.; Peng, Q.; Wang, D. S.; Li, Y. D. Single-atom catalysts: Synthetic strategies and electrochemical applications. *Joule* **2018**, *2*, 1242–1264.

[19] Lefèvre, M.; Proietti, E.; Jaouen, F.; Dodelet, J. P. Iron-based catalysts with improved oxygen reduction activity in polymer electrolyte fuel cells. *Science* **2009**, *324*, 71–74.

[20] Qu, Y. T.; Li, Z. J.; Chen, W. X.; Lin, Y.; Yuan, T. W.; Yang, Z. K.; Zhao, C. M.; Wang, J.; Zhao, C.; Wang, X. et al. Direct transformation of bulk copper into copper single sites via emitting and trapping of atoms. *Nat. Catal.* **2018**, *1*, 781–786.

[21] Han, Y. H.; Wang, Y. G.; Xu, R. R.; Chen, W. X.; Zheng, L. R.; Han, A. J.; Zhu, Y. Q.; Zhang, J.; Zhang, H. B.; Luo, J. et al. Electronic structure engineering to boost oxygen reduction activity by controlling the coordination of the central metal. *Energy Environ. Sci.* **2018**, *11*, 2348–2352.

[22] Pan, Y.; Lin, R.; Chen, Y. J.; Liu, S. J.; Zhu, W.; Cao, X.; Chen, W. X.; Wu, K. L.; Cheong, W. C.; Wang, Y. et al. Design of single-atom Co-N₅ catalytic site: A robust electrocatalyst for CO₂ reduction with nearly 100% CO selectivity and remarkable stability. *J. Am. Chem. Soc.* **2018**, *140*, 4218–4221.

[23] He, L.; Weniger, F.; Neumann, H.; Beller, M. Synthesis, characterization, and application of metal nanoparticles supported on nitrogen-doped carbon: Catalysis beyond electrochemistry. *Angew. Chem., Int. Ed.* **2016**, *55*, 12582–12594.

[24] Xiong, Y.; Sun, W. M.; Han, Y. H.; Xin, P. Y.; Zheng, X. S.; Yan, W. S.; Dong, J. C.; Zhang, J.; Wang, D. S.; Li, Y. D. Cobalt single atom site catalysts with ultrahigh metal loading for enhanced aerobic oxidation of ethylbenzene. *Nano Res.*, in press, DOI: 10.1007/s12274-020-3244-4.

[25] Schwob, T.; Kempe, R. A reusable Co catalyst for the selective hydrogenation of functionalized nitroarenes and the direct synthesis of imines and benzimidazoles from nitroarenes and aldehydes. *Angew. Chem., Int. Ed.* **2016**, *55*, 15175–15179.

[26] Zhou, P.; Jiang, L.; Wang, F.; Deng, K. J.; Lv, K. L.; Zhang, Z. H. High performance of a cobalt-nitrogen complex for the reduction and reductive coupling of nitro compounds into amines and their derivatives. *Sci. Adv.* **2017**, *3*, e1601945.

[27] Liu, W. G.; Zhang, L. L.; Liu, X.; Liu, X. Y.; Yang, X. F.; Miao, S.; Wang, W. T.; Wang, A. Q.; Zhang, T. Discriminating catalytically active FeNₓ species of atomically dispersed Fe-N-C catalyst for selective oxidation of the C–H bond. *J. Am. Chem. Soc.* **2017**, *139*, 10790–10798.

[28] Wang, X. Q.; Chen, Z.; Zhao, X. Y.; Yao, T.; Chen, W. X.; You, R.; Zhao, C. M.; Wu, G.; Wang, J.; Huang, W. X. et al. Regulation of coordination number over single Co sites: Triggering the efficient electroreduction of CO₂. *Angew. Chem., Int. Ed.* **2018**, *57*, 1944–1948.

[29] Li, X. Y.; Rong, H. P.; Zhang, J. T.; Wang, D. S.; Li, Y. D. Modulating the local coordination environment of single-atom catalysts for enhanced catalytic performance. *Nano Res.* **2020**, *13*, 1842–1855.

[30] Zafar, Z.; Ni, Z. H.; Wu, X.; Shi, Z. X.; Nan, H. Y.; Bai, J.; Sun, L. T. Evolution of Raman spectra in nitrogen doped graphene. *Carbon* **2013**, *61*, 57–62.

[31] Luo, W.; Wang, B.; Heron, C. G.; Allen, M. J.; Morre, J.; Maier, C. S.; Stickle, W. F.; Ji, X. L. Pyrolysis of cellulose under ammonia leads to nitrogen-doped nanoporous carbon generated through methane formation. *Nano Lett.* **2014**, *14*, 2225–2229.

[32] Liu, J. W.; Webster, S.; Carroll, D. L. Temperature and flow rate of NH₃ effects on nitrogen content and doping environments of carbon nanotubes grown by injection CVD method. *J. Phys. Chem. B* **2005**, *109*, 15769–15774.

[33] Liu, W. G.; Chen, Y. J.; Qi, H. F.; Zhang, L. L.; Yan, W. S.; Liu, X. Y.; Yang, X. F.; Miao, S.; Wang, W. T.; Liu, C. G. et al. A durable nickel single-atom catalyst for hydrogenation reactions and cellulose valorization under harsh conditions. *Angew. Chem., Int. Ed.* **2018**, *57*, 7071–7075.

[34] Chen, W.; Yang, H. P.; Chen, Y. Q.; Xia, M. W.; Chen, X.; Chen, H. P. Transformation of nitrogen and evolution of n-containing species during algae pyrolysis. *Environ. Sci. Technol.* **2017**, *51*, 6570–6579.

[35] Wei, L. H.; Wen, L. N.; Yang, T. H.; Zhang, N. Nitrogen transformation during sewage sludge pyrolysis. *Energy Fuels* **2015**, *29*, 5088–5094.

[36] Li, J.; Wang, Z. Y.; Yang, X.; Hu, L.; Liu, Y. W.; Wang, C. X. Evaluate the pyrolysis pathway of glycine and glycylglycine by TG-FTIR. *J. Anal. Appl. Pyrol.* **2007**, *80*, 247–253.

[37] Chen, C. M.; Zhang, Q.; Zhao, X. C.; Zhang, B. S.; Kong, Q. Q.; Yang, M. G.; Yang, Q. H.; Wang, M. Z.; Yang, Y. G.; Schlögl, R. et al. Hierarchically aminated graphene honeycombs for electrochemical capacitive energy storage. *J. Mater. Chem.* **2012**, *22*, 14076–14084.

[38] Khusnutdinova, J. R.; Milstein, D. Metal-ligand cooperation. *Angew. Chem., Int. Ed.* **2015**, *54*, 12236–12273.

[39] Colpas, G. J.; Maroney, M. J.; Bagyinka, C.; Kumar, M.; Willis, W. S.; Suib, S. L.; Mascharak, P. K.; Baidya, N. X-ray spectroscopic studies of nickel complexes, with application to the structure of nickel sites in hydrogenases. *Inorg. Chem.* **1991**, *30*, 920–928.

[40] Grosvenor, A. P.; Biesinger, M. C.; Smart, R. S. C.; McIntyre, N. S. New interpretations of XPS spectra of nickel metal and oxides. *Surf. Sci.* **2006**, *600*, 1771–1779.

[41] Yang, H. B.; Hung, S. F.; Liu, S.; Yuan, K. D.; Miao, S.; Zhang, L. P.; Huang, X.; Wang, H. Y.; Cai, W. Z.; Chen, R. Atomically dispersed Ni(I) as the active site for electrochemical CO_2 reduction. *Nat. Energy* **2018**, *3*, 140–147.

[42] Yang, L.; Cheng, D. J.; Xu, H. X.; Zeng, X. F.; Wan, X.; Shui, J. L.; Xiang, Z. H.; Cao, D. P. Unveiling the high-activity origin of single-atom iron catalysts for oxygen reduction reaction. *Proc. Natl. Acad. Sci. USA* **2018**, *115*, 6626–6631.

[43] Yang, F.; Wang, M. J.; Liu, W.; Yang, B.; Wang, Y.; Luo, J.; Tang, Y. S.; Hou, L. Q.; Li, Y.; Li, Z. et al. Atomically dispersed Ni as the active site towards selective hydrogenation of nitroarenes. *Green Chem.* **2019**, *21*, 704–711.

[44] Wang, Y. L.; Shi, R.; Shang, L.; Waterhouse, G. I. N.; Zhao, J. Q.; Zhang, Q. H.; Gu, L.; Zhang, T. R. High-efficiency oxygen reduction to hydrogen peroxide catalyzed by nickel single-atom catalysts with tetradentate N_2O_2 coordination in a three-phase flow cell. *Angew. Chem., Int. Ed.* **2020**, *59*, 13057–13062.

[45] Li, J. K.; Jiao, L.; Wegener, E.; Richard, L. L.; Liu, E. S.; Zitolo, A.; Sougrati, M. T.; Mukerjee, S.; Zhao, Z. P.; Huang, Y. et al. Evolution pathway from iron compounds to $Fe_1(II)$-N_4 sites through gas-phase iron during pyrolysis. *J. Am. Chem. Soc.* **2020**, *142*, 1417–1423.

[46] Shimizu, K. I.; Miyamoto, Y.; Satsuma, A. Size- and support-dependent silver cluster catalysis for chemoselective hydrogenation of nitroaromatics. *J. Catal.* **2010**, *270*, 86–94.

[47] Chen, B.; Dingerdissen, U.; Krauter, J. G. E.; Lansink Rotgerink, H. G. J.; Möbus, K.; Ostgard, D. J.; Panster, P.; Riermeier, T. H.; Seebald, S.; Tacke, T. et al. New developments in hydrogenation catalysis particularly in synthesis of fine and intermediate chemicals. *Appl. Catal. A Gen.* **2005**, *280*, 17–46.

[48] Corma, A.; Serna, P. Chemoselective hydrogenation of nitro compounds with supported gold catalysts. *Science* **2006**, *313*, 332–334.

[49] Chen, Y. J.; Gao, R.; Ji, S. F.; Li, H. J.; Tang, K.; Jiang, P.; Hu, H. B.; Zhang, Z. D.; Hao, H. G.; Qu, Q. Y. et al. Atomic-level modulation of electronic density at cobalt single-atom sites derived from metal–organic frameworks: Enhanced oxygen reduction performance. *Angew. Chem., Int. Ed.* **2021**, *60*, 3212–3221.

[50] Rong, X.; Wang, H. J.; Lu, X. L.; Si, R.; Lu, T. B. Controlled synthesis of a vacancy-defect single-atom catalyst for boosting CO_2 electroreduction. *Angew. Chem., Int. Ed.* **2020**, *59*, 1961–1965.

[51] Yan, C. C.; Li, H. B.; Ye, Y. F.; Wu, H. H.; Cai, F.; Si, R.; Xiao, J. P.; Miao, S.; Xie, S. H.; Yang, F. et al. Coordinatively unsaturated nickel–nitrogen sites towards selective and high-rate CO_2 electroreduction. *Energy Environ. Sci.* **2018**, *11*, 1204–1210.

[52] Tomishige, K.; Nakagawa, Y.; Tamura, M. Selective hydrogenolysis and hydrogenation using metal catalysts directly modified with metal oxide species. *Green Chem.* **2017**, *19*, 2876–2924.

[53] Niu, J.; Rao, B. K.; Jena, P. Binding of hydrogen molecules by a transition-metal ion. *Phys. Rev. Lett.* **1992**, *68*, 2277–2280.